ADVANCED ENERGY MATERIALS
www.advenergymat.de

Surface Plasmon and Scattering-Enhanced Low-Bandgap Polymer Solar Cell by a Metal Grating Back Electrode

Jingbi You, Xuanhua Li, Feng-xian Xie, Wei E. I. Sha, Johnson H. W. Kwong, Gang Li, Wallace C. H. Choy, and Yang Yang**

Polymer solar cells hold the promise for a cost-effective, lightweight solar energy conversion platform, which can benefit from simple solution processing of the active layer.[1–3] At present, bulk hetero-junction polymer solar cells show power conversion efficiency (PCE) close to or over than 8%.[4–10] However, the quantum efficiency of polymer solar cells is mainly limited due to the comparatively low carrier mobility and charge recombination.[1–3] A thinner active layer can lower the probability of charge recombination and increase the carrier drift velocity by having higher electric field, thus enhancing the internal quantum efficiency, while a minimum film thickness is always required to ensure sufficient photon absorption.[11,12] Therefore, how to increase the light absorption of a polymer film at a limited thickness of film still remains as a challenge. The incorporation of plasmonic structures with photovoltaic devices has been shown to increase solar cell photo-current and may lead to new opportunities for inexpensive, and high efficiency solar cell designs.[13–20] Recently, metallic nanostructures have been introduced into thin inorganic semiconductor solar cells (e.g. Si and GaAs solar cells) for highly efficient light harvesting by strong light scattering behavior and concentrated near field through the localized and surface plasmonic effects of different metallic nanostructures.[12–17] More recently, metallic nanostructures have been used to enhance the performance of bulk heterojunction polymer solar cells, such as introducing the localized plasmonic nanostructure of metallic nanoparticles (NPs) in carrier transport layer,[18–22] incorporate into active layer of bulk junctions,[23–25] both carrier transport layer and active layer[26] and most of them are concentrated on wide band-gap polymer, such as poly-3(hexylthiophene) (P3HT). Importantly, low bandgap polymer can cover a broad absorption range, it is therefore attractive if we can enhance the PCE of low bandgap polymer solar cell by plasmonic structure. In this study, the low bandgap polymer benzodithiophene polymers (PTB7)[6] is used to demonstrate the surface plasmonic effects of large-area metallic grating on patterned active layer. By patterning the active layer via a simple imprinting technique[26–29] and coating metal oxide/Ag, grating electrode is introduced to enhance optical properties of polymer solar cells. For a strict comparison, we firstly optimize the unpatterned polymer solar cell structures. About 10% of short current density improvement is obtained, and PCE achieves 7.73% for the plasmonic inverted solar cells with the low-bandgap polymer as the active layer. An observable improvement in PCE is mainly ascribed by the surface plasmonic and scattering effects due to the Ag grating.

To demonstrate surface plasmonic effects in low bandgap polymer solar cell, high performance PTB7 was adopted due to its broad absorption.[6] In this study, inverted structure based polymer solar cells were used to demonstrate plasmonic effects. The device structure is ITO/ZnO nanoparticles (NPs)/PTB7:$PC_{71}BM$/MoO_3/Ag, where the thickness of ZnO, active layer, MoO_3 and Ag are 30 nm, 100 nm, 8 nm and 100 nm, respectively. The ZnO nanoparticles function as an electron transport layer (ETL), the thin MoO_3 layer has dual roles of a hole transport layer (HTL) and a buffer layer to avoid carrier recombination due to direct contact between the metal and active layer. It is worthy to note that the thin MoO_3 layer can favor the plasmonic coupling between the active layer and Ag electrode. Since the surface of active layer is usually very smooth due to its excellent phase separation, and the surface roughness is lower than 5 nm, it is very hard to excite surface plasmon due to momentum mismatch.[14,30]

To introduce surface plasmonic effects in solar cells, we propose to pattern the active layer by simple imprinting technique, and then metal oxide/metal are coated on the active layer to form metal nano-grating for back contact electrode. The grating structures can also fulfill the momentum matching conditions through the Floquet (Bloch) modes supported in periodic structure (the theoretical studies will be detailed later), and can be utilized to excite surface plasmons. The scheme of the patterned devices is shown in **Figure 1**. Firstly, ZnO NPs and active layer were spin coated in sequence on glass/ITO substrate in succession, and then polydimethylsiloxane (PDMS) pattern were layered on active layer. After imprinting, the pattern was lifted off and then MoO_3/Ag film was deposited on the active layer to form metal grating. For realizing an effective coupling of the very strong near field of surface plasmon resonances from metallic grating into the active layer, the thickness of MoO_3 should be thin enough. Meanwhile, a certain thickness of MoO_3 layer is needed such that the MoO_3 layer to function as a buffer layer for eliminating the direct contact between metal and active layer. Consequently, in this study, 8 nm thickness of MoO_3 is used for fulfilling these requirements simultaneously.

Dr. J. B. You, Dr. G. Li, Prof. Y. Yang
Department of Material Science and Engineering
University of California
Los Angeles, CA 90095, USA
E-mail: yangy@ucla.edu
X. H. Li, F.-x. Xie, W. E. I. Sha, J. H. W. Kwong, Prof. W. C. H. Choy
Department of Electrical and Electronic Engineering
The University of Hong Kong
Pokfulam Road, Hong Kong
E-mail: chchoy@eee.hku.hk

DOI: 10.1002/aenm.201200108

© 2012 WILEY-VCH Verlag GmbH & Co. KGaA, Weinheim

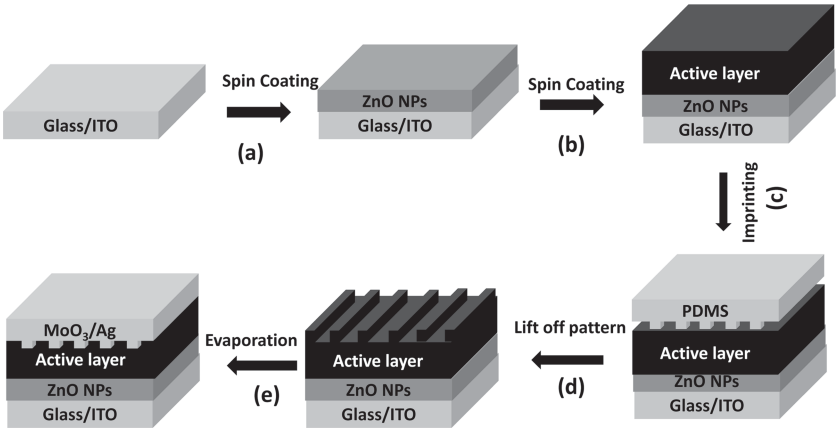

Figure 1. The scheme of patterned polymer solar cells, (a) spin coating ZnO nanoparticles on ITO substrate, (b) spin coating active layer on ZnO nanoparticles, (c) imprinting PDMS pattern on active layer, (d) Lift off PDMS pattern, and (e) deposited MoO_3 (8 nm)/Ag (100 nm) on active layer to form metal grating.

In order to study the morphology change of the active layer before and after patterning, atomic force microscopy (AFM) measurement has been carried out for active layers before and after patterning, and the images are shown in **Figure 2**(a) and (b), respectively. It can be clearly seen that a pattern has been formed on the surface of the active layer after the imprinting process. The three dimensional images of the active layer before and after patterning are also shown in Figures 2(c) and (d), respectively. It can be found that the active layer are very smooth before patterning and the roughness is less than 5 nm, while the grating with width and height of 700 and 40 nm, respectively, are formed after imprinting. For comparison, the AFM image of PDMS template pattern is shown in Figure S1, the width and height of the template pattern is about 700 and 80 nm, respectively, indicating the pattern has been successfully transferred onto the active layer. It should be noted that the height (40 nm) of transferred pattern is very suitable for demonstrating surface plasmonic effect devices. It is because, firstly, the height is smaller than the active layer thickness (~100 nm), our pattern will not lead to short-circuit for the devices. Secondly, combined with the virtue of the thin metal oxide layer, metal film coating will duplicate the morphology of the active layer pattern to form metal grating for excitation of surface plasmon.

To illustrate the effects of the metal grating on the performance of polymer solar cells, the current density versus voltage (J–V) characteristics of the solar cells were taken under AM1.5G 100 mW cm^{-2} illumination as shown in **Figure 3**(a), and photovoltaic parameters are listed in **Table 1**. As shown from the result, after patterning the active layer, the short current density (J_{SC}) of the devices enhance significantly from 14.05 to 15.50 mA/cm^2, in which the enhancement ratio is as high as 10%. Consequently, the PCE increases from 7.20 to 7.73%. These results have been confirmed by reproducing experiments. To our knowledge, this is the first time for observing the obvious J_{SC} and PCE enhancement in high performance low bandgap solar cells with metal grating. In order to study the effect of short current enhancement, the external quantum efficiency (EQE) of the device with and without pattern are measured, and the corresponding results are shown in Figure 3(b), it can be found that the EQE significantly improves, and the maximum EQE increases from 65% to 70% at about 620 nm (it should be noted that the short-circuit current measured under the irradiation of sun simulator and integrated from EQE is within the rational error). The EQE enhancement ratio before and after patterning is also plotted in Figure 3(b) to distinguish which part contributed to the enhancement, it can be seen the EQE enhancement cover all the range from 350–800 nm, and the larger enhancement located at around 350, 420 and 770 nm.

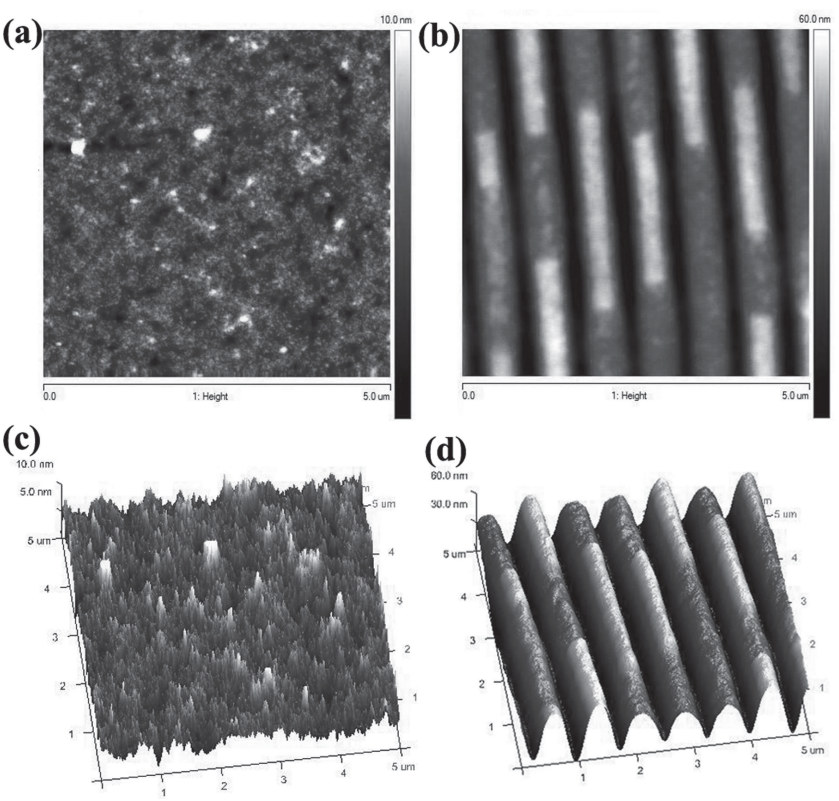

Figure 2. Atomic force microscopy (AFM) images of active layer (a) before pattering and (b) after pattering, the 3D images of active layer (c) before pattering and (d) after pattering.

As we known, the EQE is determined by two parts, including absorption and internal quantum efficiency (IQE). To further verify the reasons of EQE enhancement, firstly, the absorption spectrum (extracted from

© 2012 WILEY-VCH Verlag GmbH & Co. KGaA, Weinheim
Adv. Energy Mater. 2012,
DOI: 10.1002/aenm.201200108

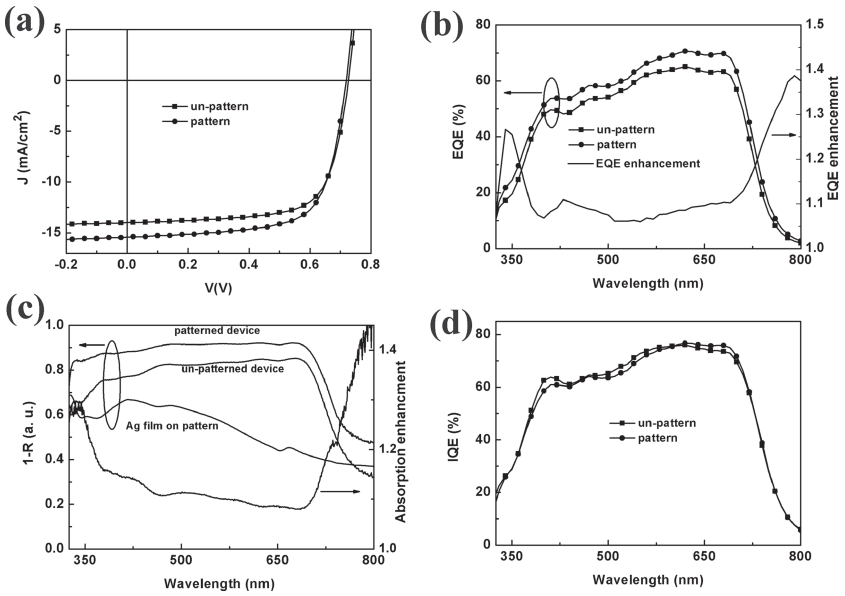

Figure 3. (a) The current density versus voltage (*J*–*V*) characteristics of the solar cell were taken under AM1.5G 100 mW cm^{-2} illumination, (b) External quantum efficiency (EQE) of the devices with and without pattern, and EQE enhancement, (c) Reflected absorption spectra of the devices with and without pattern, Ag film on PDMS pattern, and absorption enhancement, and (d) Internal quantum efficiency of the devices with and without pattern.

reflection spectrum (R) by 1–R) of the devices with and without are shown in Figure 3(c), and it is considered that the absorption is mainly from the active layer. It can be found that the device absorption significantly enhances after patterning, and the maximum absorption improves from 80% to 90%. The absorption enhancement ratio is also plotted in Figure 3(c). We can see that the enhanced absorption covers the wavelength range from 350 nm to 800 nm, and the enhancement peaks locate at around 350 nm, 420 nm and 770 nm which are consistent with EQE enhancement. These similar behaviors between EQE and absorption indicate that the EQE enhancement comes from absorption enhancement. To explore the original possibility of absorption enhancement, the absorption (1-R) of Ag film deposited on pattern is measured and the results are also shown in Figure 3(c). The main peak is 425 nm, and the other two peaks around 350 nm and 700 nm. To carefully eliminate the grating effect itself, the reflection of PDMS pattern is also measured and the results can be found in the Figure S2. It is found that the PDMS pattern only shows an absorption peak at 370 nm. Therefore, the absorption features of Ag grating on PDMS pattern are the intrinsic features from Ag grating itself. It should be noted that the 1-R peak of the Ag film on PDMS pattern at 700 nm is due to surface plasmonic resonance. After fabrication of device, due to the change of optical environment, we obtain surface plasmonic resonance at around 770 nm as shown in Figure 3(c).

In order to investigate whether IQE has any contribution to the EQE enhancement, the IQE data have been deduced from EQE and reflected absorption shown in Figures 3(b) and (c), respectively, and the results are shown in Figure 3(d). It can be found that the IQE curve are similar before and after patterning, indicating the EQE enhancement after patterning are mainly from absorption enhancement. Considering the absorption enhancement peak is very consistent with the Ag grating reflection peak, inferring that absorption enhancement is due to the effect of silver grating due to plasmonic and scattering effects. We also conduct theoretically studies on the optical effects of the polymer solar cells with Ag grating. The modeled results show that experimental EQE (absorption) enhancement peak (in Figure 3) at 350 nm is due to waveguide mode.[32] The enhancement at around 425 nm is due to Wood's anomaly which can be characterized from the peak of power flux along the grating,[31] the simulated near field distribution at 425 nm is shown in **Figure 4**(a). The enhancement peak at about

Table 1. The devices performance with and without pattern.

Devices	V_{oc} [V]	J_{sc} [mA/cm^2]	FF [%]	PCE [%]
Un-patterned	0.726	14.05	70.62	7.20
Patterned	0.720	15.50	69.08	7.73

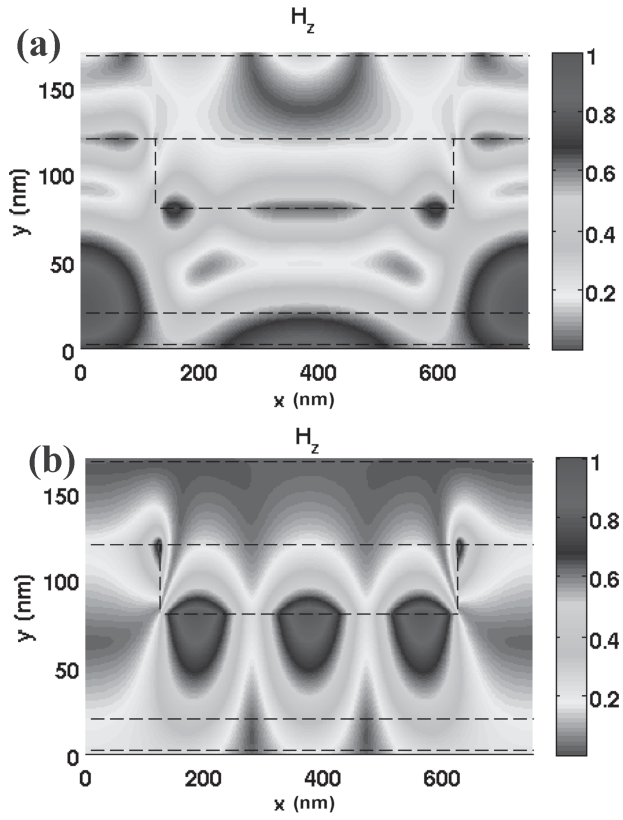

Figure 4. Simulated near field distribution of metal grating at (a) 425 nm and (b) 770 nm.

© 2012 WILEY-VCH Verlag GmbH & Co. KGaA, Weinheim

770 nm is due to surface plasmon resonance. The resonance near field profile is also shown in Figure 4(b). Consequently, we can well demonstrate and explain the EQE enhancement both experimentally and theoretically.

In conclusion, we have successfully demonstrated a highly efficient surface plasmonic low bandgap polymer solar cell by simply imprinting active layer. The introduction of plasmonic metal grating back contact electrode improves the PCE of the low bandgap solar cell from 7.20 to 7.73%. Experimental and theoretical results show that the enhancement effect is attributed from local near field enhancement and scattering effect. These results show that surface plasmonic metal nanostructures have great potential in the application of polymer solar cells. The proposed grating structures as an open platform can be applied to various polymer materials and open up the opportunities for highly efficient solar cells.

Experimental Section

Device Fabrication: The device architecture of the patterned solar cell is shown in Figure 1. The solar cells were fabricated on ITO-coated glass substrates, with sheet resistance of 15 Ω/□. The pre-cleaned ITO substrates were treated with UV-ozone. The ZnO nanoparticles was spin coated on ITO surface, and the thickness of ZnO is about 30 nm, and then active layer with PTB7 blended with $PC_{71}BM$ at a 1:1.5 weight ratio in 1% CB solution added with 3% DIO was spin-casted at 2500 rpm for 30 s on top of a layer of ZnO film. After spin coating active layer, for patterned device, then PDMS pattern was slightly covered on active layer, and after evacuation in vaccum chamber for 1–2 h, the PDMS pattern was lifted off, and the active layer with pattern will be formed. And then un-patterned and pattered devices are both sent to vacuum chamber for MoO_3/Ag back electrode evaporation.

Characterization of Photovoltaic Cells and Thin Films: The refractive index (n) and extinction coefficient (k) of PTB7:$PC_{71}BM$ were measured as shown in SI, Figure S3 by using a VASE ellipsometer from J. A.Woollam Co., Inc. The ellipsometer is operated with the antoretarder. The light source we used is a Xeon Arc lamp and the incident angle to the samples is adjusted to 65°, 70° and 75°. The diameter of the light spot is about 0.8 mm. *J–V* characteristics of photovoltaic cells were taken using a Keithley 4200 source unit under a simulated AM1.5G spectrum with an Oriel 9600 solar simulator. Absorption spectra were taken using a Varian Cary 50 ultraviolet–visible spectrophotometer. Atomic force microscopy (AFM) images were taken on a digital instruments multi-mode scanning probe microscope. External quantum efficiencies were measured using a lock-in amplifier (SR830, Stanford Research Systems) with current preamplifier (SR570, Stanford Research Systems) under short-circuit conditions. The devices were illuminated by monochromatic light from a xenon lamp passing through a monochromator (SpectraPro-2150i, Acton Research Corporation) with a typical intensity of 10 μW. The photocurrent signal is then amplified by SR570 and detected with SR830. A calibrated monosilicon diode with known spectral response is used as a reference.

Theoretical Calculation: The rigorous and efficient model has been developed for the metal grating polymer solar cells based on the rigorous electromagnetic theory through finite difference frequency domain (FDFD) approach with the staggered grids.[31] In modeling, the frequency-dependent refractive index measured experimentally of materials are used. The model is used for theoretically studying surface plasmonic resonances of a metal layer with periodic 2D nanogroove pattern in a polymer device structure. We can also discretize the boundary conditions through one-sided difference technique to achieve high accuracy. Through this model, we are able to capture not just surface PR modes, but also any possible waveguide modes and floquet modes etc in the device structures. Therefore, we can investigate their effects on the absorption of the active polymer-blends. It should be noted that the oxide buffers such as ZnO and MoO_3 layer are only a few nanometer and they are typically transparent in the considered wavelength regions, they do not have any significant effect on the surface plasmonic resonances.

Supporting Information

Supporting Information is available from the Wiley Online Library or from the author.

Acknowledgements

J.B.Y. and X.H.L. contributed equally to this work. The authors would like to thank Dr. Seiichiro Murase for helping in AFM measurements. This work was financially supported by the National Science Foundation (NSF), Air Force Office of Scientific Research (AFOSR), and Office of Naval Research (ONR). The project is also supported in part by of the grants (Nos. 712010 and 10401466) from the Research Grant Council of the Hong Kong Special Administrative Region, China and the University Grant Council (UGC) of the University of Hong Kong respectively. This project is also partially supported by a Hong Kong UGC Special Equipment Grant (SEG HKU09).

Received: February 11, 2012
Revised: April 23, 2012
Published online:

[1] K. M. Coakley, M. D. McGehee, *Chem. Mater.* **2004**, *16*, 4533.
[2] C. J. Brabec, N. S. Sariciftci, J. C. Hummelen, *Adv. Funct. Mater.* **2001**, *11*, 15.
[3] B. C. Thompson, J. M. Frechet, *Angew. Chem. Int. Ed.* **2008**, *47*, 58.
[4] L. T. Dou, J. B. You, J. Yang, C. C. Chen, Y. J. He, S. Murase, T. Moriarty, K. Emery, G. Li, Y. Yang, *Nat. Photonics* **2012**, *6*, 180.
[5] H. Y. Chen, J. H. Hou, S. Q. Zhang, Y. Y. Liang, G. W. Yang, Y. Yang, L. P. Yu, Y. Wu, G. Li, *Nat. Photonics* **2009**, *3*, 649.
[6] Y. Y. Liang, Z. Xu, J. B. Xia, S. T. Tsai, Y. Wu, G. Li, C. Ray, L. P. Yu, *Adv. Mater.* **2010**, *22*, E135.
[7] Z. C. He, C. M. Zhong, X. Huang, W. Y. Wong, H. B. Wu, L. W. Chen, S. J. Su, Y. Cao, *Adv. Mater.* **2011**, *23*, 4636.
[8] C. E. Small, S. Chen, J. Subbiah, C. M. Amb, S. W. Tsang, T. H. Lai, J. R. Reynold, F. So, *Nat. Photonics* **2012**, *6*, 115.
[9] H. X. Zhou, L. Q. Yang, A. C. Stuart, S. C. Price, S. B. Liu, W. You, *Angew. Chem. Int. Ed.* **2011**, *50*, 2995–98.
[10] T. Y. Chu, J. P. Lu, S. Beaupre, Y. G. Zhang, J. R. Pouliot, S. Wakim, J. Y. Zhou, M. Leclerc, Z. Li, J. F. Ding, Y. Tao, *J. Am. Chem. Soc.* **2011**, *133*, 4250.
[11] K. Tvingstedt, N. K. Persson, O. Inganas, A. Rahachou, I. V. Zozoulenko, *Appl. Phys. Lett.* **2007**, *91*, 113514.
[12] F. J. Beck, A. Polman, K. R. Catchpole, *J. Appl. Phys.* **2009**, *105*, 114310.
[13] J. N. Munday, H. A. Atwater, *Nano Lett.* **2011**, *11*, 2195.
[14] R. A. Pala, J. White, E. Barnard, J. Liu, M. L. Brongersma, *Adv. Mater.* **2009**, *21*, 3504.
[15] K. R. Catchpole, A. Polman, *Appl. Phys. Lett.* **2008**, *93*, 191113.
[16] V. E. Ferry, L. A. Sweatlock, D. Pacidici, H. A. Atwater, *Nano Lett.* **2008**, *8*, 4391–4397.
[17] K. Nakayama, K. Tanabe, H. A. Atwater, *Appl. Phys. Lett.* **2008**, *93*, 121904.
[18] A. J. Morfa, K. L. Rowlen, T. H. Reilly, M. J. Romero, J. van de Lagemaat, *Appl. Phys. Lett.* **2008**, *92*, 013504.
[19] F. C. Chen, J. L. Wu, C. L. Lee, Y. Hong, C. H. Kuo, M. H. Huang, *Appl. Phys. Lett.* **2009**, *95*, 013305.

© 2012 WILEY-VCH Verlag GmbH & Co. KGaA, Weinheim

[20] J. L. Wu, F. C. Chen, Y. S. Hsiao, F. C. Chen, P. L. Chen, C. H. Kuo, M. H. Huang, C. S. Hsu, *ACS Nano* **2011**, *5*, 959.
[21] D. D. S. Fung, L. Qiao, W. C. H. Choy, C. C. D. Wang, W. E. I. Sha, F. X. Xie, S. He, *J. Mater. Chem.* **2011**, *21*, 16349.
[22] J. Yang, J. B. You, C. C. Chen, W. C. Hsu, H. R. Tan, X. W. Zhang, Z. R. Hong, Y. Yang, *ACS Nano* **2011**, *5*, 6210.
[23] D. H. Wang, D. Y. Kim, K. W. Choi, J. H. Seo, S. H. Im, J. H. Park, O. O. Park, A. J. Heeger, *Angew. Chem. Int. Ed.* **2011**, *50*, 5519.
[24] C. C. D. Wang, W. C. H. Choy, C. Duan, D. D. S. Fung, W. E. I. Sha, F. X. Xie, F. Huang, Y. Cao, *J. Mater. Chem.* **2012**, *22*, 1206.
[25] A. P. Kulkarni, K. M. Noone, K. Munechika, S. R. Guyer, D. S. Ginger, *Nano Lett.* **2010**, *10*, 1501.
[26] F. X. Xie, W. C. H. Choy, C. C. D. Wang, W. E. I. Sha, D. D. S. Fung, *Appl. Phys. Lett.* **2011**, *99*, 153304.
[27] A. Williamson, E. McClean, D. Leipold, D. Zerulla, E. Runge, *Appl. Phys. Lett.* **2011**, *99*, 093307.
[28] S. I. Na, S. S. Kim, S. S. Kwon, J. Jo, J. Kim, T. Lee, D. Y. Kim, *Appl. Phys. Lett.* **2007**, *91*, 173509.
[29] J. K. Pandey, M. Aljada, M. Velusamy, P. L. Burn, P. Meredith, *Adv. Mater.* **2012**, *24*, 1055.
[30] W. L. Barnes, A. Dereux, T. W. Ebbesen, *Nature* **2003**, *424*, 824.
[31] W. E. I. Sha, W. C. H. Choy, W. C. Chew, *Opt. Express* **2010**, *18*, 5993.
[32] W. E. I. Sha, W. C. H. Choy, W. C. Chew, *Opt. Lett.* **2011**, *36*, 478.

© 2012 WILEY-VCH Verlag GmbH & Co. KGaA, Weinheim